HHS Public Access

Author manuscript

Biochim Biophys Acta. Author manuscript; available in PMC 2018 February 01.

Published in final edited form as:

Biochim Biophys Acta. 2017 February ; 1859(2): 257–267. doi:10.1016/j.bbamem.2016.11.012.

Distinct membrane properties are differentially influenced by cardiolipin content and acyl chain composition in biomimetic membranes

Edward Ross Pennington[a,b], **Amy Fix**[a], **E. Madison Sullivan**[a,b], **David A. Brown**[c], **Anthony Kennedy**[d], and **Saame Raza Shaikh**[a,b,*]

[a]Department of Biochemistry & Molecular Biology, Brody School of Medicine, East Carolina University, 115 Heart Drive, Mail Stop 743, Greenville, NC 27834, USA

[b]East Carolina Diabetes & Obesity Institute, Brody School of Medicine, East Carolina University, 115 Heart Drive, Mail Stop 743, Greenville, NC 27834, USA

[c]Department of Human Nutrition, Foods, and Exercise, Virginia Tech Corporate Research Center, 1035 ILSB, 1981 Kraft Drive, Blacksburg, VA 24060, USA

[d]Department of Chemistry, East 10th Street, Mail Stop 552, East Carolina University, Greenville, NC 27854, USA

Abstract

Cardiolipin (CL) has a critical role in maintaining mitochondrial inner membrane structure. In several conditions such as heart failure and aging, there is loss of CL content and remodeling of CL acyl chains, which are hypothesized to impair mitochondrial inner membrane biophysical organization. Therefore, this study discriminated how CL content and acyl chain composition influenced select properties of simple and complex mitochondrial mimicking model membranes. We focused on monolayer excess area/molecule (a measure of lipid miscibility), bilayer phase transitions, and microdomain organization. In monolayer compression studies, loss of tetralinoleoyl [$(18:2)_4$] CL content decreased the excess area/molecule. Replacement of $(18:2)_4$CL acyl chains with tetraoleoyl [$(18:1)_4$] CL or tetradocosahexaenoyl [$(22:6)_4$] CL generally had little influence on monolayer excess area/molecule; in contrast, replacement of $(18:2)_4$CL acyl chains with tetramyristoyl [$(14:0)_4$] CL increased monolayer excess area/molecule. In bilayers, calorimetric studies showed that substitution of $(18:2)_4$CL with $(18:1)_4$CL or $(22:6)_4$CL lowered the phase transition temperature of phosphatidylcholine vesicles whereas $(14:0)_4$CL had no effect. Finally, quantitative imaging of giant unilamellar vesicles revealed differential effects of CL

*Corresponding Author S. Raza Shaikh, 115 Heart Drive, Mail Stop 743, Greenville, NC 27834, USA, shaikhsa@ecu.edu, (252) 744-2585.

Author contributions. E.R.P. designed experiments, conducted studies, analyzed data, and wrote the manuscript; A.F. conducted experiments and analyzed data, wrote some parts of the methods; D.B. designed experiments, wrote parts of the manuscript, and provided intellectual expertise; E.M.S. conducted studies, analyzed data; A.K. designed experiments, conducted studies, analyzed data; S.R.S. designed experiments, analyzed data, wrote parts of the manuscript, and assumes responsibility for the entire project.

content and acyl chain composition on microdomain organization, visualized with the fluorescent probe Texas Red DHPE. Notably, microdomain areas were decreased by differing magnitudes upon lowering of $(18:2)_4$CL content and substitution of $(18:2)_4$CL with $(14:0)_4$CL or $(22:6)_4$CL. Conversely, exchanging $(18:2)_4$CL with $(18:1)_4$CL increased microdomain area. Altogether, these data demonstrate that CL content and fatty acyl composition differentially target membrane physical properties, which has implications for understanding how CL regulates mitochondrial activity and the design of CL-specific therapeutics.

Graphical abstract

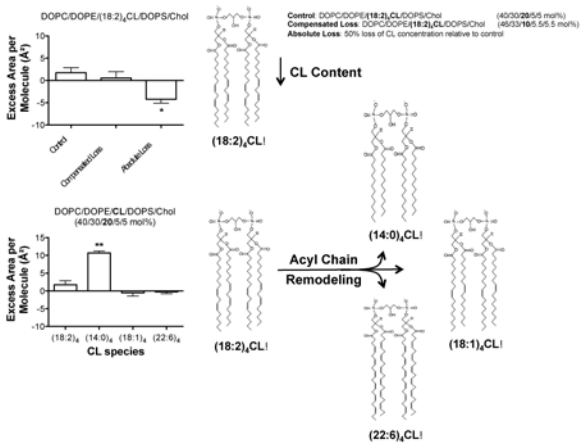

Keywords

Cardiolipin; pressure-area isotherms; docosahexaenoic acid; monolayers; mitochondria

1.0 Introduction

Cardiolipin (CL) 1 is a unique anionic phospholipid that consists of two phosphatidic acid moieties linked by a central glycerol. CL is predominately localized and synthesized in the inner mitochondrial membrane where it plays an important role in mitochondrial fusion/fission, apoptosis, cellular signaling, and electron transport [1-4]. CL interacts with proteins of the inner mitochondrial membrane, especially respiratory chain complexes and substrate carriers during oxidative phosphorylation [5-7]. Furthermore, it is hypothesized that CL, due to its ability to form non-bilayer structures, forms local microdomains, which may be essential for the formation of highly curved cristae [8;9]. Therefore, CL has a critical role in regulating mitochondrial membrane structure and thereby function.

In conditions like aging or pathologies such as cancers, diabetes, cardiac diseases, Parkinson's, and Barth syndrome, CL undergoes considerable changes [10-21]. Three well-

[1]Abbreviations: 1,1′,2,2′-tetra-(4Z,7Z,10Z,13Z,16Z,19Z-docosahexaenoyl) cardiolipin [$(22:6)_4$CL], 1,1′,2,2′-tetra-(9Z-octadecenoyl) cardiolipin [$(18:1)_4$CL], 1,1′,2,2′-tetratetradecanoyl cardiolipin [$(14:0)_4$CL], 1,2-di-(9Z-octadecenoyl)-sn-glycero-3-phosphocholine (DOPC), 1,2-di-(9Z-octadecenoyl)-sn-glycero-3-phosphoethanolamine (DOPE), 1,2-di-(9Z-octadecenoyl)-sn-glycero-3-phospho-L-serine (DOPS), 1,2-dihexadecanoyl-sn-glycero-3-phosphocholine (DPPC), bovine heart cardiolipin [$(18:2)_4$CL], cardiolipin (CL), cholesterol (Chol), differential scanning calorimetry (DSC), docosahexaenoic acid (DHA), elasticity modulus (C_S^{-1}), excess area/molecule (A_{ex}), giant unilamellar vesicle (GUV), Gibbs free energy of mixing (ΔG_{mix}), surface pressure (π).

identified pathological alterations to CL include the loss of CL content, peroxidation, and remodeling of acyl chains [10;12;15;22]. Loss of CL content could arise from either enhanced CL degradation, due to an up-regulation in phospholipase activity, or by a decrease in *de novo* synthesis as a result of compromised functions of the enzymes involved in CL synthesis [10;11]. Many of the pathological consequences associated with changes in CL content are hypothesized to be driven by a loss of CL, particularly tetralinoloeyl [$(18:2)_4$] CL that is highly abundant in tissues such as the heart [10;11]. For instance, in cardiac ischemia-reperfusion injury, CL concentration is decreased by up to 50% [23].

Aberrant CL acyl chain remodeling may arise from decreased availability of $(18:2)_4$CL and/or abnormal alterations in the specific activity of remodeling enzymes such as tafazzin [10;12;13]. CL remodeling events are highly diverse. For example, in the streptozotocin model of diabetes, a loss of $(18:2)_4$CL acyl chains is accompanied by an increase in the abundance of docosahexaenoyl (DHA, 22:6) acyl chains, which could presumably render the mitochondrial membrane more susceptible to oxidative damage [22]. Similarly, in aging, DHA acyl chains are elevated in rat heart CL in addition to increased abundance of arachidonic acid and decreased availability of linoleic acid [24].

The aforementioned changes in CL abundance and/or acyl chain composition would presumably influence the biophysical organization of lipid molecules in the inner mitochondrial membrane. Indeed, several studies show CL content regulates microviscosity, packing, morphology, and phase behavior in isolated mitochondria and model membranes [25-34]. In contrast, no lab has completely discriminated the effects of CL concentration compared to CL acyl chain remodeling on membrane organization. This is essential since there is debate in the field about the importance of CL acyl chain composition on mitochondrial function [35]. Thus, the objective of this study was to investigate select membrane properties of monolayers and bilayers in response to lowering of $(18:2)_4$CL content and replacement of 18:2 acyl chains with other fatty acids. The approach relied on model membranes, which provide the advantage of tightly controlling lipid composition [36].

2.0 Materials and Methods

2.1 Materials

Bovine heart cardiolipin [$(18:2)_4$CL)], 1,1′,2,2′-tetratetradecanoyl cardiolipin [$(14:0)_4$CL], 1,1′,2,2′-tetra-(9Z-octadecenoyl) cardiolipin [$(18:1)_4$CL], 11,2-dihexadecanoyl-sn-glycero-3-phosphocholine (DPPC), 1,2-di-(9Z-octadecenoyl)-sn-glycero-3-phosphocholine (DOPC), 1,2-di-(9Z-octadecenoyl)-sn-glycero-3-phosphoethanolamine (DOPE), 1,2-di-(9Z-octadecenoyl)-sn-glycero-3-phospho-L-serine (DOPS) and cholesterol (Chol) were purchased from Avanti Polar Lipids (Alabaster, AL). 1,1′,2,2′-tetra-(4Z,7Z,10Z,13Z,16Z, 19Z-docosahexaenoyl) cardiolipin [$(22:6)_4$CL] was a custom synthesis from Avanti Polar Lipids. All solvents were HPLC grade and purchased from Fisher Scientific (Hampton, NH). Fresh stocks of lipid mixtures were used to minimize oxidation and handling of lipids occurred under low light conditions and a gentle stream of nitrogen gas.

2.2 Generation of monolayers

Pressure-area isotherms were generated on a Mini Langmuir-Blodgett Trough (KSV NIMA, Biolin Scientific, Paramus, NJ) using a Wilhelmy plate at a compression rate of 3.0 mm/min. Lipid mixtures were spotted using a Hamilton syringe and spread on a subphase of 10 mM sodium phosphate buffer (pH 7.4). Trough barriers were compressed and expanded prior to spotting lipids until the surface pressure remained constant (<0.3 mN/m). Compression began 10 minutes after spotting the lipids to ensure evaporation of chloroform. The trough was washed three times with 70% ethanol, Milli-Q water, and subphase prior to collecting pressure-area isotherms.

Lipid monolayers containing differing levels of CL were composed of either a binary mixture of DPPC and CL, or heterogeneous mixtures of DOPC, DOPE, CL, DOPS, and Chol. The amounts of PC, PE, CL, PS, and Chol approximated ratios found in cardiac inner mitochondrial membranes in health and disease [37]. All lipid mixtures were acquired multiple times to ensure reproducibility.

2.3 Analysis of lipid miscibility, elasticity modulus, and Gibbs free energy of mixing in monolayers

The ideal mean molecular area of multi-component mixed monolayers was calculated at a constant surface pressure (**π**) by:

$$A_{\text{ideal}}=X_1(A_1)_\pi+X_2(A_2)_\pi+\ldots X_n(A_n)_\pi \quad \text{(Eq. 1)}$$

where X_n represents the mol fraction of each individual component and A_n represents the mean molecular area of each component [38]. The excess area/molecule (A_{ex}), a measurement of lipid miscibility, was calculated at a given surface pressure (**π**) by [39-41]:

$$A_{\text{ex}}=(A_{12\ldots n})_\pi-(X_1A_1+X_2A_2+\ldots X_nA_n)_\pi \quad \text{(Eq. 2)}$$

where X_n represents the mol fraction of each individual component and A_n represents the mean molecular area of each component. ($A_{12\ldots n}$) represents the mean molecular area of the mixed monolayer of interest at a given surface pressure (**π**). A negative excess area/molecule indicates attractive forces and a positive excess area/molecule indicates repulsive forces [39]. The surface pressure-area isotherms were also used to calculate the surface elasticity modulus (C_s^{-1}):

$$C_s^{-1}=(-A)(d\pi/dA)_\pi \quad \text{(Eq. 3)}$$

where A is the mean molecular area of the lipid mixture of interest at the indicated surface pressure (**π**). Gibbs free energy of mixing (ΔG_{mix}) was determined by the following relation:

$$\Delta G_{\mathrm{mix}}=\Delta G_{\mathrm{ex}}+\Delta G_{\mathrm{ideal}} \quad \text{(Eq. 4)}$$

where ΔG_{ex} represents the excess Gibbs free energy of mixing and ΔG_{ideal} is the ideal Gibbs free energy of mixing. ΔG_{ex} was calculated from the pressure-area isotherms using the following expression [39]:

$$\Delta G_{\mathrm{ex}}=\int_0^{\pi}[A_{12\ldots n}-(X_1A_1+X_2A_2+X_nA_n)]d\pi \quad \text{(Eq. 5)}$$

where A_n and X_n are the mean molecular area and mol fraction of each component, respectively, at a given surface pressure (π). ΔG_{ideal} was calculated from:

$$\Delta G_{\mathrm{ideal}}=RT(X_1lnX_1+X_2lnX_2+X_nlnX_n) \quad \text{(Eq. 6)}$$

where R represents the ideal gas constant, T represents the temperature in Kelvin, and X_n represents the mol fraction of each component.

2.4 Differential scanning calorimetry (DSC)

Lipid mixtures of DPPC and CL (5.0 mg total lipid) were co-dissolved in chloroform and dried under nitrogen gas. Excess chloroform was removed by vacuum pumping in the dark overnight. Each sample was hydrated for one hour with frequent vortex mixing in 10 mM sodium phosphate buffer (pH 7.4) at ~55 °C. The lipid suspension was subjected to three freeze-thaw cycles and then extruded using a mini extruder (Avanti Polar Lipids, Alabaster, AL). Each sample was extruded at ~55 °C for a total of 15 passes across a 1.0 micron polycarbonate membrane (Whatman Nuclepore, Clifton, NJ).

A total of 0.30 mg of each lipid mixture was placed in hermetically sealed aluminum T-zero pans (TA Instruments, New Castle, DE). DSC curves were obtained using a TA Instruments Q2000 DSC (TA Instruments, New Castle, DE). Samples were subjected to one heating cycle (20 °C to 60 °C) immediately followed by one cooling cycle (60 °C to 20 °C) at a scan rate of 2 °C per minute. Each sample was analyzed against a reference pan containing 10 mM sodium phosphate buffer (pH 7.4). Raw DSC curves were analyzed using TA Universal Analysis 2000 software as previously described (TA Instruments, New Castle, DE) [42].

2.5 Construction of giant unilamellar vesicles (GUVs)

GUVs were constructed by electroformation as described [43;44]. Lipids (37.5 mol% DPPC, 27.4 mol% DOPC, 25 mol% Chol, 10 mol% CL) and the fluorescent probe Texas Red DHPE (0.1 mol%; Life Technologies, Carlsbad, CA) were co-dissolved in chloroform to achieve a total concentration of 0.5 mg/ml [45]. Next, 7.5 μg of total lipid was spread onto the conductive side of an indium tin oxide coated glass slide. The lipid-coated slide was

subjected to vacuum pumping in the dark for 3 hours to remove excess solvent. Once the lipid film was dried, a GUV electroformation chamber was assembled as described [44].

GUV electroformation was performed at ~55 °C, in the dark, using a 250 mM sucrose solution. GUV electroformation frequency and peak-to-peak voltage was controlled using a HP3324A programmable function generator. Initially, a sine waveform with a frequency of 10 Hz and a peak-to-peak voltage ranging from 0.2 V to 1.4 V was applied and linearly increased over a 30 minute period. Next, a sine waveform with a frequency of 10 Hz and a peak-to-peak voltage of 1.4 V was applied and held constant for 120 minutes. For the detachment of GUVs, a square waveform with a frequency of 4.5 Hz and peak-to-peak voltage of 2.1 V was applied and held constant for 30 minutes. Once electroformation was completed, GUVs were extracted from the chamber using a 20½-gauge needle and refrigerated (4 °C) overnight prior to imaging. GUVs were drawn into a rectangular micro-capillary tube, mounted onto a microscope slide, and imaged at room temperature (23 °C).

2.6 Confocal microscopy and image analysis

Imaging was conducted using an Olympus FV1000 Confocal Microscope using a 60× 1.35NA oil immersion objective (Olympus, Waltham, MA). Analysis of microdomains was conducted with NIH ImageJ as previously described [46;47]. After background subtraction, membrane microdomains were quantified as the area occupied by the fluorophore Texas Red DHPE, which reports on disordered microdomains [48-50]. A range of microdomain areas were measured and are presented as a frequency distribution. A Gaussian fit (Graph Pad Prism v5.0b) was applied to the frequency distributions. Larger areas reflect greater coverage of the fluorophore on the perimeter of the GUV. The diameter of each GUV was quantified using NIH ImageJ.

2.7 Statistics

Data were analyzed with GraphPad Prism v5.0b. Data were ensured to display normalized distributions. Statistical significance relied on one-way ANOVA followed by a post-hoc Bonferroni test compared to $(18:2)_4$CL. For select GUV studies, statistical analyses were conducted with a one-way ANOVA followed by a post-hoc Bonferroni multiple comparison test. P values less than 0.05 were considered significant.

3.0 Results

3.1 Monolayers of differing CL species in DPPC/CL and DOPC/DOPE/CL/DOPS/Chol mixtures

The behavior of four different CL species (Fig. S1A-D, Supporting Material) was studied in DPPC/CL and DOPC/DOPE/CL/DOPS/Chol monolayers. The rationale for using the DPPC/CL model system was to allow for comparison with previous studies with binary mixtures containing CL [33;34;51]. The five-component mixture (PC/PE/CL/PS/Chol) modeled what is more biologically relevant for mitochondrial inner membranes. The first objective was to specifically understand how loss of $(18:2)_4$CL content and replacement of $(18:2)_4$CL with other CL species would influence monolayer properties.

We present the raw monolayer data, which were then used to generate quantitative values on excess area/molecule, elasticity modulus, and Gibbs free energy of mixing. Sample monolayers of DPPC/CL with increasing levels of $(18:2)_4$CL, $(14:0)_4$CL, $(18:1)_4$CL, and $(22:6)_4$CL are depicted in Figure 1A-D. All four CL species alone occupied a much greater mean molecular area compared to DPPC alone, which was in agreement with the notion that CL is a larger structure than DPPC. At high surface pressures, $(18:2)_4$CL notably displayed a long plateau region suggesting possible expulsion of $(18:2)_4$CL from the monolayer (Fig. 1A). $(14:0)_4$CL displayed a unique isotherm with a plateau region around 20 mN/m (Fig. 1B). In contrast, $(18:1)_4$CL (Fig. 1C) and $(22:6)_4$CL (Fig. 1D) did not have any plateau regions. Decreasing the levels of any of the CLs in DPPC/CL monolayers, which occurred at the expense of increasing DPPC, decreased the mean molecular area at all surface pressures (Fig. 1A-D).

Figure 2A-D respectively presents sample monolayers of DOPC/DOPE/CL/DOPS/Chol with differing mol percent of $(18:2)_4$CL, $(14:0)_4$CL, $(18:1)_4$CL, and $(22:6)_4$CL. CL concentration was increased at the expense of the other lipids (for simplicity referred to as 'compensated loss'); thus, as CL levels increased, the levels of DOPC/DOPE/DOPS/Chol were reduced. Pressure-area isotherms for all four CL species showed one clear trend; decreasing the levels of CL in the DOPC/DOPE/CL/DOPS/Chol system decreased the mean molecular area (Fig. 2A-D).

Monolayers of DPPC/$(18:2)_4$CL (80/20 mol%) were also generated in which $(18:2)_4$CL concentration was reduced by 50%, referred to as an 'absolute loss' of CL (Fig. S2A, Supporting Material). As expected, an absolute loss of $(18:2)_4$CL content in DPPC/$(18:2)_4$CL monolayers decreased the mean molecular area relative to DPPC/$(18:2)_4$CL (80/20 mol%) (Fig. S2A, Supporting Material). Similarly, monolayers of DOPC/DOPE/$(18:2)_4$CL/DOPS/Chol (40/30/20/5/5 mol%) were generated in which $(18:2)_4$CL concentration was lowered by 50%, again referred to as an 'absolute loss' of CL (Fig. S2B, Supporting Material). The absolute loss of $(18:2)_4$CL content in DOPC/DOPE/$(18:2)_4$CL/DOPS/Chol monolayers did not have a dramatic effect on the pressure-area isotherms, displaying a small decrease in the mean molecular area (Fig. S2B, Supporting Material).

3.2 Loss of $(18:2)_4$CL content promotes a decrease in the excess area/molecule with modest effects on the elasticity modulus

The aforementioned pressure-area isotherms (Figs. 1-2 & Fig. S2 Supporting Material) were used to calculate the excess area/molecule, the elasticity modulus (C_s^{-1}), and the Gibbs free energy of mixing (ΔG_{mix}) in response to a loss of $(18:2)_4$CL content and changes in CL acyl chain composition. All analyses were conducted at a physiologically relevant surface pressure of 30 mN/m [52;53].

DPPC/$(18:2)_4$CL (80/20 mol%) and DOPC/DOPE/$(18:2)_4$CL/DOPS/Chol (40/30/20/5/5 mol %) were defined as the control (Fig. 3A, Table 1). Compensated loss of $(18:2)_4$CL (i.e. increase in DPPC at the expense of lowering CL) had no influence on the excess area/molecule (Fig. 3A left panel, Table 1). An absolute loss of $(18:2)_4$CL content (i.e. 50% loss of CL concentration) decreased the excess area/molecule by 11.0 $Å^2$ in DPPC/$(18:2)_4$CL monolayers relative to the control (Fig. 3A left panel, Table 1). Similarly, in DOPC/DOPE/

$(18:2)_4$CL/DOPS/Chol monolayers, compensated loss of $(18:2)_4$CL (i.e. increase in DOPC/DOPE/DOPS/Chol at the expense of lowering CL) had no influence on excess area/molecule (Fig. 3A right panel, Table 1). An absolute loss of $(18:2)_4$CL content (i.e. 50% loss of CL concentration) in DOPC/DOPE/$(18:2)_4$CL/DOPS/Chol monolayers decreased the excess area/molecule by 6.0 $Å^2$ relative to the control (Fig. 3A right panel, Table 1).

Elasticity modulus (C_s^{-1}) values were not affected by compensated loss of $(18:2)_4$CL but were lowered by 11.1 mN/m with the absolute loss of $(18:2)_4$CL content in DPPC/$(18:2)_4$CL monolayers (Fig. 3B left panel, Table 1). Compensated or absolute loss of $(18:2)_4$CL content had no influence on C_s^{-1} values of DOPC/DOPE/$(18:2)_4$CL CL/DOPS/Chol monolayers (Fig. 3B right panel, Table 1). The formation of both DPPC/$(18:2)_4$CL (Fig. 3C left panel, Table 1) and DOPC/DOPE/$(18:2)_4$CL/DOPS/Chol monolayers (Fig. 3C right panel, Table 1) showed negative values for the Gibbs free energy of mixing. Gibbs free energy of mixing was lowered with the compensated and absolute loss of $(18:2)_4$CL compared to the control in DPPC/$(18:2)_4$CL monolayers (Fig. 3C left panel, Table 1).

3.3 Replacement of $(18:2)_4$CL with $(18:1)_4$CL or $(22:6)_4$CL has no effect on excess area/molecule in model mitochondrial monolayers with the exception of $(14:0)_4$CL

CL undergoes remodeling of its acyl chains, particularly to 22:6, in conditions such as heart failure or aging [12;22;24;54]. Therefore, the different CL species were compared in the DPPC/CL (80/20 mol%) (Fig. 4, left panel) and DOPC/DOPE/CL/DOPS/Chol (40/30/20/5/5 mol%) (Fig. 4, right panel) monolayer models. $(14:0)_4$CL showed a significant increase in the excess area/molecule in both model systems by approximately 4.1 $Å^2$ and 8.9 $Å^2$, respectively, compared to $(18:2)_4$CL (Fig. 4A left and right panels, Table 2). The $(22:6)_4$CL species decreased the excess area/molecule by 6.2 $Å^2$ compared to $(18:2)_4$CL in the DPPC/CL system (Fig. 4A left panel, Table 2) but had no effect in the model mitochondrial monolayers of DOPC/DOPE/CL/DOPS/Chol (Fig. 4A right panel, Table 2). Replacement of $(18:2)_4$CL with $(18:1)_4$CL had no effect on area/molecule in either model system (Fig. 4A left and right panels, Table 2).

C_s^{-1} values were significantly elevated by 2.8-fold with $(14:0)_4$CL compared to $(18:2)_4$CL in the DPPC/CL mixture (Fig. 4B left panel, Table 2). $(18:1)_4$CL and $(22:6)_4$CL had no effect on C_s^{-1} of DPPC/CL monolayers (Fig. 4B left panel, Table 2). In the DOPC/DOPE/CL/DOPS/Chol monolayers, $(14:0)_4$CL and $(18:1)_4$CL very modestly increased C_s^{-1} values, whereas $(22:6)_4$CL decreased C_s^{-1} compared to $(18:2)_4$CL (Fig. 4B right panel, Table 2). Gibbs free energy of mixing values were all negative for DPPC/CL (Fig. 4C left panel, Table 2) and DOPC/DOPE/CL/DOPS/Chol (Fig. 4C right panel, Table 2) monolayers. Replacement of $(18:2)_4$CL with the other CL species in the DPPC/CL monolayers led to a decrease in the Gibbs free energy of mixing, but overall the quantity remained negative (Fig. 4C left panel, Table 2).

3.4 At low levels of CL, replacement of $(18:2)_4$CL with $(18:1)_4$CL or $(22:6)_4$CL has no effect on excess area/molecule in model mitochondrial monolayers with the exception of $(14:0)_4$CL

We next addressed how exchange of $(18:2)_4$CL with the other CL species would influence area/molecule, elasticity modulus, and Gibbs free energy at a low CL concentration. In DOPC/DOPE/CL/DOPS/Chol (48/35/5/6/6 mol%) (Fig. S3A left panel, Supporting Material), $(14:0)_4$CL modestly increased the excess area/molecule with no statistically significant effect with the other CL species compared to $(18:2)_4$CL. In DOPC/DOPE/CL/DOPS/Chol (46/33/10/5.5/5.5 mol%) monolayers (Fig. S3A, right panel, Supporting Material), there were no differences between the CL species on excess area/molecule. Both $(18:1)_4$CL and $(22:6)_4$CL lowered C_s^{-1} values by 14.0 mN/m and 22.6 mN/m, respectively, in DOPC/DOPE/CL/DOPS/Chol (48/35/5/6/6 mol%) compared to the $(18:2)_4$CL control (Fig. S3B left panel, Supporting Material). In DOPC/DOPE/CL/DOPS/Chol (46/33/10/5.5/5.5 mol%) monolayers containing $(18:1)_4$CL and $(22:6)_4$CL, C_s^{-1} values were lowered by 10.5 mN/m and 18.4 mN/m, respectively (Fig. S3B right panel, Supporting Material). Gibbs free energy of mixing was negative for all lipid mixtures (Fig. S3C, left and right panels, Supporting Material).

3.5 In Bilayers, Replacement Of $(18:2)_4$Cl With $(18:1)_4$Cl Or $(22:6)_4$Cl Decreases The Phase Transition Temperature Of Dppc With The Exception Of $(14:0)_4$Cl

We further investigated if differing CL species, upon addition to DPPC bilayers, had differential effects on the phase transition temperature, cooperativity, and enthalpies of DPPC using DSC. DSC heating scans of lipid vesicles showed that the addition of increasing amounts of $(18:2)_4$CL (5-20 mol%) (Fig. 5A) decreased the main phase transition (T_m, centered at 41.6 °C), cooperativity ($T_{m1/2}$), and enthalpy (ΔH) for DPPC (Table 3). In contrast, addition of $(14:0)_4$CL to DPPC had no major effect on the main phase transition temperature (Fig. 5B). Enthalpy values were lowered with increasing amounts of $(14:0)_4$CL to DPPC to a much smaller degree compared to $(18:2)_4$CL (Fig. 5B, Table 3). Both $(18:1)_4$CL (Fig. 5C) and $(22:6)_4$CL (Fig. 5D) qualitatively and quantitatively (Table 3) showed similar effects as $(18:2)_4$CL on the main phase transition temperature, cooperativity, and enthalpy of DPPC. No major hysteresis was observed given that analyses of DSC cooling scans showed similar results (data not shown).

3.6 Loss of $(18:2)_4$CL content and remodeling to $(14:0)_4$CL have a stronger influence on lipid microdomain organization than remodeling to $(18:1)_4$ or $(22:6)_4$CL

Finally, we assessed how CL content and acyl chain composition influenced lipid microdomain organization, a key biophysical parameter of membranes. In order to understand how different CL species would organize lipid microdomains, we employed a model membrane system of DPPC/DOPC/Chol that is well known to form phase separated microdomains [45]. The fluorescent probe Texas Red DHPE was used to image the organization of microdomains. Microdomains were visible in GUVs made of DPPC/DOPC/Chol/$(18:2)_4$CL (37.5/27.4/25/10 mol%) with a broad Gaussian distribution of microdomain areas (Fig. 6A).

Replacement of $(18:2)_4$CL with $(14:0)_4$CL in the DPPC/DOPC/Chol GUVs led to an increased frequency of distinct microdomains (Fig. 6B). Frequency analysis (Fig. 6B) showed a tightening distribution with smaller microdomain areas at higher frequencies with $(14:0)_4$CL compared to $(18:2)_4$CL. $(18:1)_4$CL generally showed less phase separated microdomains compared to $(18:2)_4$CL, with domains that covered the entire perimeter of the GUVs (Fig. 6C). This was reflected by a shift to the right in the domain area distribution compared to $(18:2)_4$CL (Fig. 6C). $(22:6)_4$CL also influenced microdomain organization, although not as pronounced as $(14:0)_4$CL when compared to $(18:2)_4$CL (Fig. 6D). We also measured microdomain areas upon the lowering of $(18:2)_4$CL concentration by 50% (Fig. 6E). The frequency distribution was tight with the majority of microdomains being relatively small (Fig. 6E) compared to $(18:2)_4$CL (Fig. 6A).

The average microdomain area for each CL species in the DPPC/DOPC/Chol/CL GUVs was calculated. Relative to $(18:2)_4$CL, both $(14:0)_4$CL and $(22:6)_4$CL had decreased average microdomain areas by 3.4-fold and 1.7-fold respectively, whereas $(18:1)_4$CL had an increased microdomain area by 1.3-fold (Fig. 6F). A 50% loss of $(18:2)_4$CL concetration decreased the average microdomain area relative to $(18:2)_4$CL, $(18:1)_4$CL, and $(22:6)_4$CL by 2.5-fold, 3.3-fold, and 1.5-fold, respectively (Fig. 6F). During the course of this study, we also observed that GUVs made of $(22:6)_4$CL or those that had a 50% loss of $(18:2)_4$CL concentration had a smaller diameter compared to $(18:2)_4$CL (Fig. 6G).

4.0 Discussion

4.1 Biological consequences for lowering $(18:2)_4$CL content and replacement of $(18:2)_4$CL with other CLs in monolayer studies

CL undergoes changes in concentration and acyl chain composition in a range of diseases. For instance, individuals with Barth Syndrome display a dramatic decrease in lymphoblast $(18:2)_4$CL content accompanied by remodeling of acyl chains [13;55;56]. A wide range of acyl chains are remodeled in human and mouse models of Barth Syndrome, which include (but not limited to) changes in 16:0, 16:1, 18:0, 18:1, 18:2, 20:2, 20:3, and 22:6 [56-58]. The aforementioned changes would presumably influence key biophysical properties of membranes that regulate mitochondrial function. Therefore, we studied CL content and acyl chain composition on select membrane properties.

In the differing model systems employed, $(14:0)_4$CL consistently displayed a different behavior when compared to $(18:2)_4$CL, $(18:1)_4$CL, and $(22:6)_4$CL. In monolayers, replacement of $(18:2)_4$CL with $(14:0)_4$CL led to a positive deviation in the excess area/molecule within DPPC/CL or DOPC/DOPE/CL/DOPS/Chol. A positive value for the excess area/molecule suggests that $(14:0)_4$CL does not ideally mix with the other lipids [39]. Calorimetry studies confirmed that the addition of small amounts of $(14:0)_4$CL to DPPC lipid bilayers did not completely abolish the phase transition temperature of DPPC as effectively as the other CLs. This again suggested $(14:0)_4$CL was not mixing with DPPC compared to other CLs.

The results with $(14:0)_4$CL were not in complete agreement with X-ray diffraction studies to show that $(14:0)_4$CL is highly miscible with DPPC [59]. The discrepancy between the

studies could reflect differences in the buffers used or the surface pressures used for analyses. We relied on a surface pressure of 30 mN/m whereas the aforementioned study focused on lower surface pressures. Given that $(14:0)_4$CL is found in select bacteria but not in mammalian mitochondria [60], the biological significance is limited for human physiology. There is precedence to show the accumulation of short chain fatty acids besides $(14:0)_4$CL in yeast mutant models [61]. Perhaps, a significant increase in $(14:0)_4$CL could occur in response to dietary intervention with short chain saturated fatty acids, such as those found in coconut oil. To date, this possibility has not been investigated.

Exchange of $(18:2)_4$CL with either $(18:1)_4$CL or $(22:6)_4$CL did not strongly influence monolayer excess area/molecule and elasticity modulus. The only exception was with DPPC/CL mixtures, where $(22:6)_4$CL promoted a decrease in excess area/molecule but this effect was diminished in the more relevant DOPC/DOPE/CL/DOPS/Chol monolayers. The data with $(22:6)_4$CL were particularly surprising since we expected $(22:6)_4$CL to have a strong influence on elasticity modulus, given that DHA acyl chains, due to extensive polyunsaturation, are extremely flexible [62]. Our rationale for selecting $(22:6)_4$CL, as opposed to a CL with just one or two DHA acyl chains, was to test the most extreme example of a DHA-containing CL. Overall, $(22:6)_4$CL behaved similar to the control, whereas $(14:0)_4$CL did not, in the complex mitochondrial biomimetic monolayers.

There is precedence to show that n-3 polyunsaturated fatty acids can incorporate into CL, which may be beneficial or detrimental for mitochondrial function. In pre-clinical models, DHA and eicosapentaenoic acid (EPA, 20:5) incorporate into CL and are generally beneficial for improving metabolic outcomes associated with cardiovascular disease [63-66]. Paradoxically, DHA levels are also increased in the diabetic heart, which may have negative consequences since the fatty acid is highly oxidizable [12;22]. Therefore, future studies will determine how different heteroacid CL species containing EPA or DHA influence lipid miscibility. Furthermore, there is a need to address how mono-lysocardiolipin, saturated and monounsaturated CLs, which are associated with a range of diseases including Barth Syndrome, regulate lipid miscibility [4;67].

4.2 Loss of $(18:2)_4$CL content and remodeling to $(14:0)_4$CL have a stronger influence on microdomain organization than remodeling to $(18:1)_4$CL and $(22:6)_4$CL

It is hypothesized that distinct CL membrane microdomains may regulate protein activity and there is emerging evidence for their existence [9;68]. In *E. coli*, CL molecules form macroscopic domains in regions of high curvature, which likely support the recruitment of select proteins for regulation of bacterial division [9]. There is also some discussion of CL domains as having properties akin to lipid rafts (although this is highly debatable since cholesterol levels are low in the inner mitochondrial membranes) [69;70]. The importance of CL microdomains is of relevance during initiation of apoptosis, where caspase 8 is thought to localize to CL microdomains that would be spatially distributed at contact sites between the inner and outer mitochondrial membranes [71]. In another study, fission proteins were also reported to be associated with CL microdomains [72]. However, any conclusions about the existence of CL microdomains must account for the methodology used for isolating these membrane fractions, which may promote artifacts [73].

Given the potential importance of mitochondrial microdomains, we studied how loss of $(18:2)_4$CL content and replacement of $(18:2)_4$CL species influenced the organization of microdomains visualized with Texas Red DHPE [48-50]. We acknowledge the limitation of our experiments, which relied on raft/non-raft associated lipids and did not specifically measure CL-enriched domains. However, this model has previously been employed for assaying phase separation and thus the influence of CL on microdomain organization [72]. The data qualitatively and quantitatively demonstrate that lowering $(18:2)_4$CL content led to the formation of smaller domains on a micron scale compared to higher $(18:2)_4$CL levels. This suggests that domain size is tunable by CL levels analogous to studies on cholesterol and lipid rafts [74]. It is important to note that the loss of $(18:2)_4$CL content on microdomain size was equivalent to the effect of replacing $(18:2)_4$CL with $(14:0)_4$CL. An interpretation of these data are that replacement of $(18:2)_4$CL with $(14:0)_4$CL resembles the loss of $(18:2)_4$CL concentration.

Replacement of $(18:2)_4$CL with $(14:0)_4$CL or $(22:6)_4$CL also promoted the formation of smaller domains. In the case of $(18:1)_4$CL, there was no evidence for the formation of microdomains in the DPPC/DOPC/Chol/$(18:1)_4$CL GUVs. We speculate that this was likely due to $(18:1)_4$CL localizing to both ordered and disordered regions as reported for oleic acid containing phosphatidylethanolamines, thereby preventing macroscopic phase separation between ordered and disordered domains [75].

This study did not address the composition and properties of lipid microdomains. We tested the effects of the concentration and composition of CL on microdomain organization, which is one of many biophysical properties of membranes. Future imaging studies with a range of fluorescent probes will determine the nature of mitochondrial microdomains and their significance for mitochondrial function.

4.3. CL-protein interactions may be uniquely modified in response to changes in CL content and acyl chain composition

It is plausible that lowering of CL content and remodeling of its acyl chains would influence CL-protein interactions [55;76]. This would be relevant for numerous functions such as oxidative phosphorylation enzyme activity and regulating the degradation of CL. To exemplify, Xu *et al.* recently demonstrated that CL degradation in lymphoblasts was protected by associating with select inner membrane mitochondrial proteins whereas loss of this protection, as observed in subjects with Barth syndrome, led to increased CL degradation [55]. Moreover, monounsaturated fatty acids such as oleic acid decreased the rate of CL degradation and improved supercomplex formation [55]. Therefore, subsequent studies will need to evaluate how CL content and unsaturation regulate CL-protein interactions.

4.4 Implications for the design of mitochondrial CL-specific therapeutics

Many diseases are associated with the loss of $(18:2)_4$CL and aberrant remodeling of CL acyl chains, which leads to the loss of cristae and ultimately mitochondrial function [10]. A number of pharmaceutical approaches aimed at restoring mitochondrial bioenergetics are under pre-clinical development [77-79], and many of these implicate CL. Several cell-

permeable peptides known as SS-31/Bendavia/Elamipretide and SS-20 bind CL and have shown efficacy in improving electron transport and mitochondrial function in animal models of heart and kidney disease [80-82]. In large-animal models of heart and kidney disease, treatment with the CL-targeting peptide Elamipretide improved mitochondrial energetics, lowered ROS, and restored CL content back to non-diseased levels [83;84]. Thus, development of therapeutics directed to restore CL levels and acyl chain composition has enormous potential across numerous disorders characterized by CL abnormalities.

4.4 Conclusion

The results demonstrate that $(18:2)_4$CL content and acyl chain composition differentially influence select membrane properties in biomimetic membranes. These studies set the foundation for future experiments on how CL concentration and acyl chain composition in model mitochondrial membranes influence domain size, stability, and in turn, diffusion and clustering of mitochondrial membrane proteins. Furthermore, the results have implications for the design of CL specific therapeutics and ultimately in the study of mitochondrial proteins that depend on the surrounding lipid environment for optimal function.

Supplementary Material

Refer to Web version on PubMed Central for supplementary material.

Acknowledgments

Research was supported by NIH R01HL123647 (D.B. and S.R.S), an East-West Collaboration Award (S.R.S. and A.K.), NIH R15HL122922 (D.B. and S.R.S.), Brody Brothers Foundation Award 213147 (S.R.S.), NIH K25GM100480 (S.R.S. and P.Wang), and NIH R01AT008375 (S.R.S.).

References

1. Claypool SM, Koehler CM. The complexity of cardiolipin in health and disease. Trends Biochem Sci. 2012; 37:32–41. [PubMed: 22014644]
2. Petrosillo G, Ruggiero FM, Paradies G. Role of reactive oxygen species and cardiolipin in the release of cytochrome c from mitochondria. FASEB J. 2003; 17:2202–2208. [PubMed: 14656982]
3. Paradies G, Ruggiero FM, Petrosillo G, Quagliariello E. Peroxidative damage to cardiac mitochondria: Cytochrome oxidase and cardiolipin alterations. FEBS Lett. 1998; 424:155–158. [PubMed: 9539141]
4. Ren M, Phoon CKL, Schlame M. Metabolism and function of mitochondrial cardiolipin. Prog Lipid Res. 2014; 55:1–16. [PubMed: 24769127]
5. Schwall CT, Greenwood VL, Alder NN. The stability and activity of respiratory complex II is cardiolipin-dependent. Biochim Biophys Acta. 2012; 1817:1588–1596. [PubMed: 22575443]
6. Mileykovskaya E, Dowhan W. Cardiolipin-dependent formation of mitochondrial respiratory supercomplexes. Chem Phys Lipids. 2014; 179:42–48. [PubMed: 24220496]
7. Klingenberg M. Cardiolipin and mitochondrial carriers. Biochim Biophys Acta. 2009; 1788:2048–2058. [PubMed: 19539604]
8. Mileykovskaya E, Dowhan W. Cardiolipin membrane domains in prokaryotes and eukaryotes. Biochim Biophys Acta. 2009; 1788:2084–2091. [PubMed: 19371718]
9. Renner LD, Weibel DB. Cardiolipin microdomains localize to negatively curved regions of Escherichia coli membranes. Proc Natl Acad Sci U S A. 2011; 108:6264–6269. [PubMed: 21444798]

10. Chicco AJ, Sparagna GC. Role of cardiolipin alterations in mitochondrial dysfunction and disease. Am J Physiol. 2007; 292:C33–C44.
11. Sparagna GC, Chicco AJ, Murphy RC, Bristow MR, Johnson CA, Rees ML, Maxey ML, McCune SA, Moore RL. Loss of cardiac tetralinoleoyl cardiolip in human and experimental heart failure. J Lipid Res. 2007; 48:1559–1570. [PubMed: 17426348]
12. He Q, Han X. Cardiolipin remodeling in diabetic heart. Chem Phys Lipids. 2014; 179:75–81. [PubMed: 24189589]
13. Schlame M, Kelley RI, Feigenbaum A, Towbin JA, Heerdt PM, Schieble T, Wanders RJA, DiMauro S, Blanck TJJ. Phospholipid abnormalities in children with Barth syndrome. J Am Coll Cardiol. 2003; 42:1994–1999. [PubMed: 14662265]
14. Paradies, Giuseppe; Paradies, Valeria; Ruggiero, Francesca M.; Petrosillo, Giuseppe. Cardiolipin and mitochondrial function in health and disease Antioxid. Redox Signal. 2014:1925–1953.
15. Shen Z, Ye C, McCain K, Greenberg ML. The role of cardiolipin in cardiovascular health. BioMed Res Int. 2015; 2015:891707. [PubMed: 26301254]
16. Paradies G, Paradies V, Ruggiero FM, Petrosillo G. Cardiolipin alterations and mitochondrial dysfunction in heart ischemia/reperfusion injury. Clin Lipidol. 2015; 10:415–429.
17. Paradies G, Petrosillo G, Paradies V, Ruggiero FM. Role of cardiolipin peroxidation and Ca2+ in mitochondrial dysfunction and disease. Cell Calcium. 2009; 45:643–650. [PubMed: 19368971]
18. Julienne CM, Tardieu M, Chevalier S, Pinault M, Bougnoux P, Labarthe F, Couet C, Servais S, Dumas J. Cardiolipin content is involved in liver mitochondrial energy wasting associated with cancer-induced cachexia without the involvement of adenine nucleotide translocase. Biochim Biophys Acta. 2014; 1842:726–733. [PubMed: 24534708]
19. Kiebish MA, Han X, Cheng H, Chuang JH, Seyfried TN. Cardiolipin and electron transport chain abnormalities in mouse brain tumor mitochondria: Lipidomic evidence supporting the Warburg theory of cancer. J Lipid Res. 2008; 49:2545–2556. [PubMed: 18703489]
20. Malhotra A, Edelman-Novemsky I, Xu Y, Plesken H, Ma J, Schlame M, Ren M. Role of calcium-independent phospholipase A(2) in the pathogenesis of Barth syndrome. Proc Natl Acad Sci U S A. 2008; 106:2337–2341.
21. Tyurina YY, Winnica DE, Kapralova VI, Kapralov AA, Tyurin VA, Kagan VE. LC/MS characterization of rotenone induced cardiolipin oxidation in human lymphocytes: Implications for mitochondrial dysfunction associated with Parkinson's disease. Mol Nutr Food Res. 2013; 57:1410–1422. [PubMed: 23650208]
22. Han X, Yang J, Yang K, Zhao Z, Abendschein DR, Gross RW. Alterations in myocardial cardiolipin content and composition occur at the very earliest stages of diabetes: A shotgun lipidomics study. Biochemistry. 2007; 46:6417–6428. [PubMed: 17487985]
23. Petrosillo G, Ruggiero FM, Di Venosa N, Paradies G. Decreased complex III activity in mitochondria isolated from rat heart subjected to ischemia and reperfusion: role of reactive oxygen species and cardiolipin. FASEB J. 2003:714–716. [PubMed: 12586737]
24. Lee H, Mayette J, Rapoport SI, Bazinet RP. Selective remodeling of cardiolipin fatty acids in the aged rat heart. Lipids Health Dis. 2006; 5:2. [PubMed: 16430781]
25. Paradies G, Petrosillo G, Pistolese M, Ruggiero FM. Reactive oxygen species affect mitochondrial electron transport complex I activity through oxidative cardiolipin damage. Gene. 2002; 286:135–141. [PubMed: 11943469]
26. Paradies G, Petrosillo G, Pistolese M, Di Venosa N, Federici A, Ruggiero FM. Decrease in mitochondrial complex I activity in ischemic/reperfused rat heart: involvement of reactive oxygen species and cardiolipin. Circ Res. 2004; 94:53–59. [PubMed: 14656928]
27. Zhang M, Mileykovskaya E, Dowhan W. Cardiolipin is essential for organization of complexes III and IV into a supercomplex in intact yeast mitochondria. J Biol Chem. 2005; 280:29403–29408. [PubMed: 15972817]
28. Petrosillo G, Casanova G, Matera M, Ruggiero FM, Paradies G. Interaction of peroxidized cardiolipin with rat-heart mitochondrial membranes: Induction of permeability transition and cytochrome c release. FEBS Lett. 2006; 580:6311–6316. [PubMed: 17083938]
29. Boscia AL, Treece BW, Mohammadyani D, Klein-Seetharaman J, Braun AR, Wassenaar TA, Klösgen B, Tristram-Nagle S. X-ray structure, thermodynamics, elastic properties and MD

simulations of cardiolipin/dimyristoylphosphatidylcholine mixed membranes. Chem Phys Lipids. 2014; 178:1–10. [PubMed: 24378240]

30. Lewis RNAH, Zweytick D, Pabst G, Lohner K, McElhaney RN. Calorimetric, X-ray diffraction, and spectroscopic studies of the thermotropic phase behavior and organization of tetramyristoyl cardiolipin membranes. Biophys J. 2007; 92:3166–3177. [PubMed: 17293402]
31. Lewis RNAH, McElhaney RN. The physicochemical properties of cardiolipin bilayers and cardiolipin-containing lipid membranes. Biochim Biophys Acta. 2009; 1788:2069–2079. [PubMed: 19328771]
32. Frias M, Benesch MGK, Lewis RNAH, McElhaney RN. On the miscibility of cardiolipin with 1,2-diacyl phosphoglycerides: Binary mixtures of dimyristoylphosphatidylethanolamine and tetramyristoylcardiolipin. Biochim Biophys Acta. 2011; 1808:774–783. [PubMed: 21182822]
33. Unsay JD, Cosentino K, Subburaj Y, García-Sáez AJ. Cardiolipin effects on membrane structure and dynamics. Langmuir. 2013; 29:15878–15887. [PubMed: 23962277]
34. Phan M, Shin K. Effects of cardiolipin on membrane morphology: A Langmuir monolayer study. Biophys J. 2015; 108:1977–1986. [PubMed: 25902437]
35. Baile MG, Sathappa M, Lu Y, Pryce E, Whited K, McCaffery JM, Han X, Alder NN, Claypool SM. Unremodeled and remodeled cardiolipin are functionally indistinguishable in yeast. J Biol Chem. 2014; 289:1768–1778. [PubMed: 24285538]
36. Shaikh SR, Wassall SR, Brown DA, Kosaraju R. Chapter Six - N-3 Polyunsaturated fatty acids, lipid microclusters, and vitamin E. Curr Top Membr. 2015; 75:209–231. [PubMed: 26015284]
37. Zeczycki TN, Whelan J, Hayden WT, Brown DA, Shaikh SR. Increasing levels of cardiolipin differentially influence packing of phospholipids found in the mitochondrial inner membrane. Biochem Biophys Res Commun. 2014; 450:366–371. [PubMed: 24905496]
38. Shaikh SR, Dumaual AC, Jenski LJ, Stillwell W. Lipid phase separation in phospholipid bilayers and monolayers modeling the plasma membrane. Biochim Biophys Acta. 2001; 1512:317–328. [PubMed: 11406109]
39. Nichols-Smith S, Teh S, Kuhl TL. Thermodynamic and mechanical properties of model mitochondrial membranes. Biochim Biophys Acta. 2004; 1663:82–88. [PubMed: 15157610]
40. Domènech Ò, Sanz F, Montero MT, Hernández-Borrell J. Thermodynamic and structural study of the main phospholipid components comprising the mitochondrial inner membrane. Biochim Biophys Acta. 2006; 1758:213–221. [PubMed: 16556434]
41. Chou T, Chang C. Thermodynamic characteristics of mixed DPPC/DHDP monolayers on water and phosphate buffer subphases. Langmuir. 2000; 16:3385–3390.
42. Pennington ER, Day C, Parker JM, Barker M, Kennedy A. Thermodynamics of interaction between carbohydrates and unilamellar dipalmitoyl phosphatidylcholine membranes. J Therm Anal Calorim. 2016; 123:2611–2617.
43. Angelova MI, Soléau S, Méléard P, Faucon F, Bothorel P. Preparation of giant vesicles by external AC electric fields. Kinetics and applications. Prog Colloid Polym Sci. 1992; 89:127–131.
44. Schmid EM, Richmond DL, Fletcher DA. Chapter 17 - Reconstitution of proteins on electroformed giant unilamellar vesicles. Methods Cell Biol. 2015; 128:319–338. [PubMed: 25997355]
45. Veatch SL, Keller SL. Separation of liquid phases in giant vesicles of ternary mixtures of phospholipids and cholesterol. Biophys J. 2003; 85:3074–3083. [PubMed: 14581208]
46. Shaikh SR, Rockett BD, Salameh M, Carraway K. Docosahexaenoic acid modifies the clustering and size of lipid rafts and the lateral organization and surface expression of MHC class I of EL4 cells. J Nutr. 2009; 139:1632–1639. [PubMed: 19640970]
47. Rockett BD, Teague H, Harris M, Melton M, Williams J, Wassall SR, Shaikh SR. Fish oil increases raft size and membrane order of B cells accompanied by differential effects on function. J Lipid Res. 2012; 53:674–685. [PubMed: 22315394]
48. Baumgart T, Hunt G, Farkas ER, Webb WW, Feigenson GW. Fluorescence probe partitioning between Lo/Ld phases in lipid membranes. Biochim Biophys Acta. 2007; 1768:2182–2194. [PubMed: 17588529]
49. Juhasz J, Davis J, Sharom F. Fluorescent probe partitioning in giant unilamellar vesicles of “lipid raft” mixtures. Biochem J. 2010; 430:415. [PubMed: 20642452]

50. Klymchenko A, Kreder R. Fluorescent probes for lipid rafts: From model membranes to living cells. Chem Biol. 2014; 21:97–113. [PubMed: 24361047]
51. Joanne P, Galanth C, Goasdoué N, Nicolas P, Sagan S, Lavielle S, Chassaing G, El Amri C, Alves ID. Lipid reorganization induced by membrane-active peptides probed using differential scanning calorimetry. Biochim Biophys Acta. 2009; 1788:1772–1781. [PubMed: 19427300]
52. Seelig A. Local anesthetics and pressure: A comparison of dibucaine binding to lipid monolayers and bilayers. Biochim Biophys Acta. 1987; 899:196–204. [PubMed: 3580365]
53. Demel RA, Geurts van Kessel WSM, Zwaal RFA, Roelofsen B, van Deenen LLM. Relation between various phospholipase actions on human red cell membranes and the interfacial phospholipid pressure in monolayers. Biochim Biophys Acta. 1975; 406:97–107. [PubMed: 1174576]
54. Han X, Yang J, Cheng H, Yang K, Abendschein DR, Gross RW. Shotgun lipidomics identifies cardiolipin depletion in diabetic myocardium linking altered substrate utilization with mitochondrial dysfunction. Biochemistry. 2005; 44:16684–16694. [PubMed: 16342958]
55. Xu Y, Phoon CKL, Berno B, D'Souza K, Hoedt E, Zhang G, Neubert TA, Epand RM, Ren M, Schlame M. Loss of protein association causes cardiolipin degradation in Barth syndrome. Nat Chem Biol. 2016; 12:641–647. [PubMed: 27348092]
56. Xu Y, Sutachan JJ, Plesken H, Kelley RI, Schlame M. Characterization of lymphoblast mitochondria from patients with Barth syndrome. Lab Invest. 2005; 85:823–830. [PubMed: 15806137]
57. Kiebish MA, Yang K, Liu X, Mancuso DJ, Guan S, Zhao Z, Sims HF, Cerqua R, Cade WT, Han X, Gross RW. Dysfunctional cardiac mitochondrial bioenergetic, lipidomic, and signaling in a murine model of Barth syndrome. J Lipid Res. 2013; 54:1312–1325. [PubMed: 23410936]
58. Valianpour F, Wanders RJA, Barth PG, Overmars H, van Gennip AH. Quantitative and compositional study of cardiolipin in platelets by electrospray ionization mass spectrometry: Application for the identification of Barth syndrome patients. Clin Chem. 2002; 48:1390. [PubMed: 12194913]
59. Etienne F, Roche Y, Peretti P, Bernard S. Cardiolipin packing ability studied by grazing incidence X-ray diffraction. Chem Phys Lipids. 2008; 152:13–23. [PubMed: 18206648]
60. Hoch FL. Cardiolipins and biomembrane function. Biochim Biophys Acta. 1992; 1113:71–133. [PubMed: 1550861]
61. Rijken PJ, Houtkooper RH, Akbari H, Brouwers JF, Koorengevel MC, de Kruijff B, Frentzen M, Vaz FM, de Kroon AIPM. Cardiolipin molecular species with shorter acyl chains accumulate in saccharomyces cerevisiae mutants lacking the acyl coenzyme A-binding protein Acb1p: New insights into acyl chain remodeling of cardiolipin. J of Biol Chem. 2009; 284:27609–27619. [PubMed: 19656950]
62. Stillwell W, Wassall SR. Docosahexaenoic acid: Membrane properties of a unique fatty acid. Chem Phys Lipids. 2003; 126:1–27. [PubMed: 14580707]
63. Ting H, Chao Y, Hsu YH. Polyunsaturated fatty acids incorporation into cardiolipin in H9c2 cardiac myoblast. J Nutr Biochem. 2015; 26:769–775. [PubMed: 25866137]
64. Khairallah RJ, Sparagna GC, Khanna N, O'Shea M K, Hecker PA, Kristian T, Fiskum G, Rosiers CD, Polster BM, Stanley WC. Dietary supplementation with docosahexaenoic acid, but not eicosapentanoic acid, dramatically alters cardiac mitochondrial phospholipid fatty acid composition and prevents permeability transition. Biochim Biophys Acta. 2010; 1797:1555–1562. [PubMed: 20471951]
65. O'Shea M K, Khairallah RJ, Sparagna GC, Xu W, Hecker PA, Robillard-Frayne I, Des Rosiers C, Kristian T, Murphy RC, Fiskum G, Stanley WC. Dietary omega-3 fatty acids alter cardiac mitochondrial phospholipid composition and delay Ca(2+)-induced permeability transition. J Mol Cell Cardiol. 2009; 47:819–827. [PubMed: 19703463]
66. Shah KB, Duda MK, O'Shea M K, Sparagna GC, Chess DJ, Khairallah RJ, Robillard-Frayne I, Xu W, Murphy RC, Des Rosiers C, Stanley WC. The cardioprotective effects of fish oil during pressure overload are blocked by high fat intake: Role of cardiac phospholipid remodeling. Hypertension. 2009; 54:605–611. [PubMed: 19597033]

67. Ye C, Shen Z, Greenberg ML. Cardiolipin remodeling: A regulatory hub for modulating cardiolipin metabolism and function. J Bioenerg Biomembr. 2016; 48:113–123. [PubMed: 25432572]
68. Mukhopadhyay R, Huang KC, Wingreen NS. Lipid localization in bacterial cells through curvature-mediated microphase separation. Biophys J. 95:1034–1049.
69. Lingwood D, Simons K. Lipid rafts as a membrane-organizing principle. Science. 2009; 327:46–50.
70. Ciarlo L, Manganelli V, Matarrese P, Garofalo T, Tinari A, Gambardella L, Marconi M, Grasso M, Misasi R, Sorice M, Malorni W. Raft-like microdomains play a key role in mitochondrial impairment in lymphoid cells from patients with Huntington's disease. J Lipid Res. 2012; 53:2057–2068. [PubMed: 22773688]
71. Sorice M, Manganelli V, Matarrese P, Tinari A, Misasi R, Malorni W, Garofalo T. Cardiolipin-enriched raft-like microdomains are essential activating platforms for apoptotic signals on mitochondria. FEBS Lett. 2009; 583:2447–2450. [PubMed: 19616549]
72. Stepanyants N, Macdonald PJ, Francy CA, Mears JA, Qi X, Ramachandran R. Cardiolipin's propensity for phase transition and its reorganization by dynamin-related protein 1 form a basis for mitochondrial membrane fission. Mol Biol Cell. 2015; 26:3104–3116. [PubMed: 26157169]
73. Zheng YZ, Berg KB, Foster LJ. Mitochondria do not contain lipid rafts, and lipid rafts do not contain mitochondrial proteins. J Lipid Res. 2009; 50:988–998. [PubMed: 19136664]
74. Pollock AH, Tedla N, Hancock SE, Cornely R, Mitchell TW, Yang Z, Kockx M, Parton RG, Rossy J, Gaus K. Prolonged intake of dietary lipids alters membrane structure and T cell responses in LDLr-/- mice. J Immunol. 2016; 196:3993–4002. [PubMed: 27183636]
75. Shaikh SR, Lo Cascio DS, Soni SP, Wassall SR, Stillwell W. Oleic- and docosahexaenoic acid-containing phosphatidylethanolamines differentially phase separate from sphingomyelin. Biochim Biophys Acta. 2009; 1788:2421–2426. [PubMed: 19735642]
76. Beales PA, Bergstrom CL, Geerts N, Groves JT, Vanderlick TK. Single vesicle observations of the cardiolipin-cytochrome c interaction: Induction of membrane morphology changes. Langmuir. 2011; 27:6107–6115. [PubMed: 21504165]
77. Murphy MP. Targeting lipophilic cations to mitochondria. Biochim Biophys Acta. 2008; 1777:1028–1031. [PubMed: 18439417]
78. Walters AM, Porter GA, Brookes PS. Mitochondria as a drug target in ischemic heart disease and cardiomyopathy. Circ Res. 2012; 111:1222–1236. [PubMed: 23065345]
79. Brown DA, Sabbah HN, Shaikh SR. Mitochondrial inner membrane lipids and proteins as targets for decreasing cardiac ischemia/reperfusion injury. Pharmacol Ther. 2013; 140:258–266. [PubMed: 23867906]
80. Szeto HH. Mitochondria-targeted cytoprotective peptides for ischemia-reperfusion injury. Antioxid Redox Signal. 2008; 10:601–619. [PubMed: 17999629]
81. Birk AV, Liu S, Soong Y, Mills W, Singh P, Warren JD, Seshan SV, Pardee JD, Szeto HH. The mitochondrial-targeted compound SS-31 re-energizes ischemic mitochondria by interacting with cardiolipin. J Am Soc Nephrol. 2013; 24:1250–1261. [PubMed: 23813215]
82. Sloan RC, Moukdar F, Frasier CR, Patel HD, Bostian PA, Lust RM, Brown DA. Mitochondrial permeability transition in the diabetic heart: Contributions of thiol redox state and mitochondrial calcium to augmented reperfusion injury. J Mol Cell Cardiol. 2012; 52:1009–1018. [PubMed: 22406429]
83. Sabbah HN, Gupta RC, Kohli S, Wang M, Hachem S, Zhang K. Chronic therapy with elamipretide (MTP-131), a novel mitochondria-targeting peptide, improves left ventricular and mitochondrial function in dogs with advanced heart failure. Circ Heart Fail. 2016; 9:e002206. [PubMed: 26839394]
84. Eirin A, Ebrahimi B, Zhang X, Zhu X, Woollard JR, He Q, Textor SC, Lerman A, Lerman LO. Mitochondrial protection restores renal function in swine atherosclerotic renovascular disease. Cardiovasc Res. 2014; 103:461–472. [PubMed: 24947415]

Highlights

- In several diseases, cardiolipin (CL) content is lowered and acyl chains remodeled.
- CL content has a strong impact on physical properties of biomimetic membranes.
- Remodeling of $(18:2)_4$CL to $(14:0)_4$CL has a strong influence on membrane properties.
- $(18:2)_4$CL, $(18:1)_4$CL, and $(22:6)_4$CL behave similarly in complex monolayers.
- CL content and acyl chain composition differentially target membrane organization.

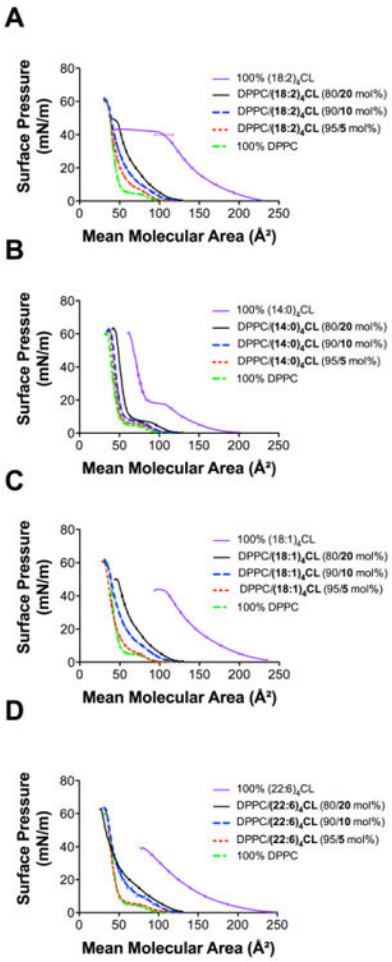

Figure 1. Monolayers containing differing CL species mixed with DPPC

Pressure-area isotherms of DPPC/CL containing differing levels of (A) $(18:2)_4$CL, (B) $(14:0)_4$CL, (C) $(18:1)_4$CL, and (D) $(22:6)_4$CL. Isotherms were acquired at 23 °C using a 10 mM sodium phosphate buffer (pH 7.4). Isotherms were used for calculating excess area/molecule, elasticity modulus, and Gibbs free energy of mixing. Data are average ± S.E.M. from 3 independent experiments.

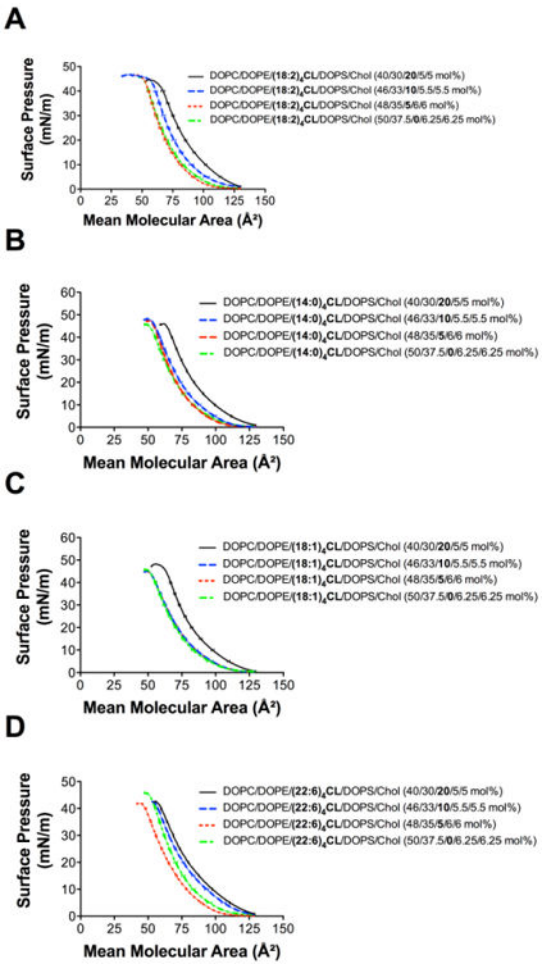

Figure 2. Monolayers containing differing CL species in model mitochondrial membranes

Pressure-area isotherms of DOPC/DOPE/CL/DOPS/Chol at varying mol percent of (A) $(18:2)_4$CL, (B) $(14:0)_4$CL, (C) $(18:1)_4$CL, and (D) $(22:6)_4$CL. Isotherms were acquired at 23 °C using a 10 mM sodium phosphate buffer (pH 7.4). Isotherms were used for calculating excess area/molecule, elasticity modulus, and Gibbs free energy of mixing. Data are average ± S.E. from 3-9 independent experiments.

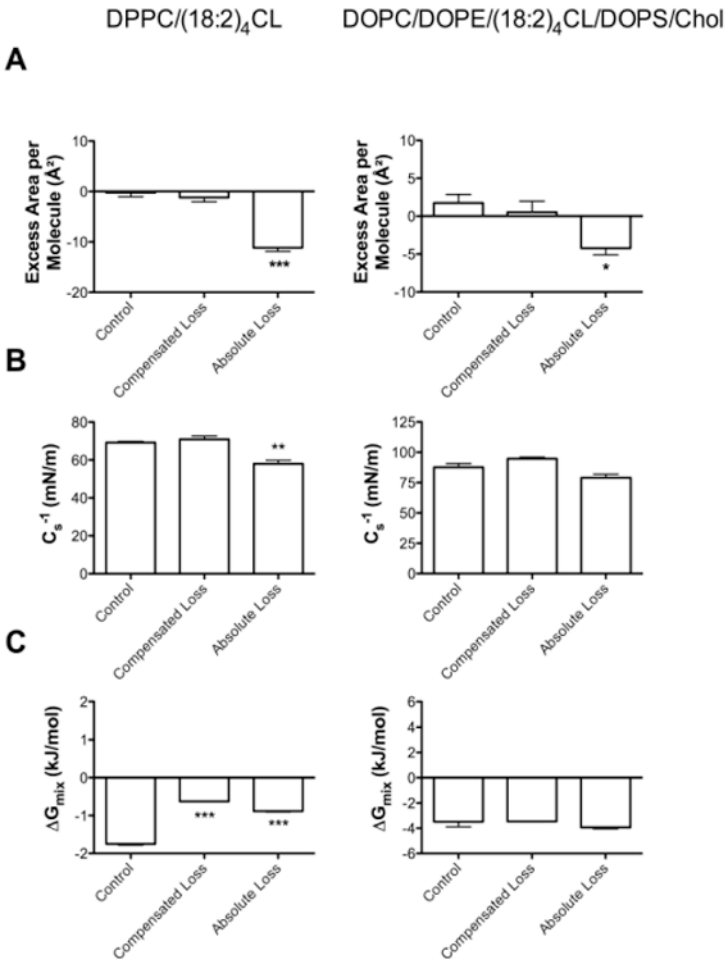

Figure 3. Loss of $(18:2)_4$CL content decreases the excess area/molecule in monolayer models

(A) Excess area/molecule, (B) elasticity modulus, and (C) Gibbs free energy of mixing for DPPC/$(18:2)_4$CL (left panel) and DOPC/DOPE/$(18:2)_4$CL/DOPS/Chol (right panel) monolayers. Values were calculated from pressure-area isotherms at a physiologically relevant surface pressure of 30 mN/m. Control samples are defined as either DPPC/$(18:2)_4$CL (80/20 mol%) or DOPC/DOPE/$(18:2)_4$CL/DOPS/Chol (40/30/20/5/5 mol%). Compensated loss is defined as a 50% loss of $(18:2)_4$CL content with a compensated increase in DPPC content or DOPC/DOPE/DOPS/Chol content. Absolute loss is defined as a 50% loss of $(18:2)_4$CL concentration. Data are average ± S.E.M. from 3-6 independent experiments. Asterisks indicate significant from the control: *P<0.05, **P<0.01, ***P<0.001.

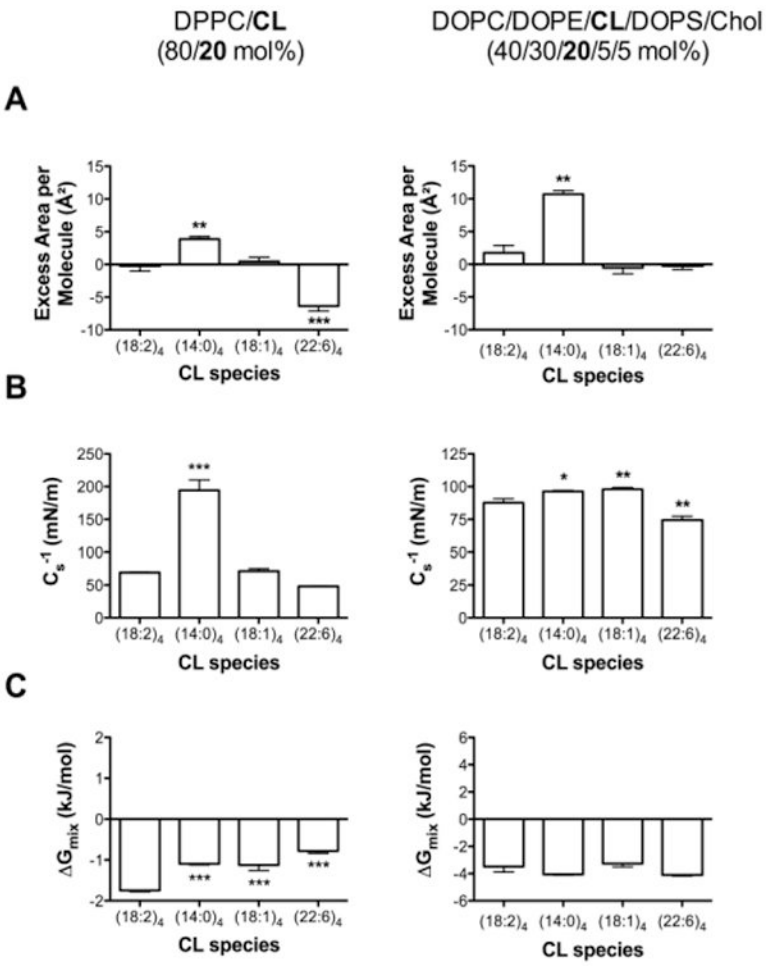

Figure 4. Replacement of $(18:2)_4$CL with other CLs differentially influences monolayer excess area/molecule, elasticity modulus, and Gibbs free energy of mixing

(A) Excess area/molecule, (B) elasticity modulus, and (C) Gibbs free energy of mixing for DPPC/CL (left panel) and DOPC/DOPE/CL/DOPS/Chol (right panel) monolayers. Values were calculated from pressure-area isotherms at a surface pressure of 30 mN/m. $(18:2)_4$CL species is defined as the control. DPPC/CL levels were maintained at 80/20 (mol%) and DOPC/DOPC/CL/DOPS/Chol levels were kept at 40/30/20/5/5 (mol%). Data are average ± S.E.M. from 3-9 independent experiments. Asterisks indicate significance from $(18:2)_4$CL: *P<0.05, **P<0.01, ***P<0.001.

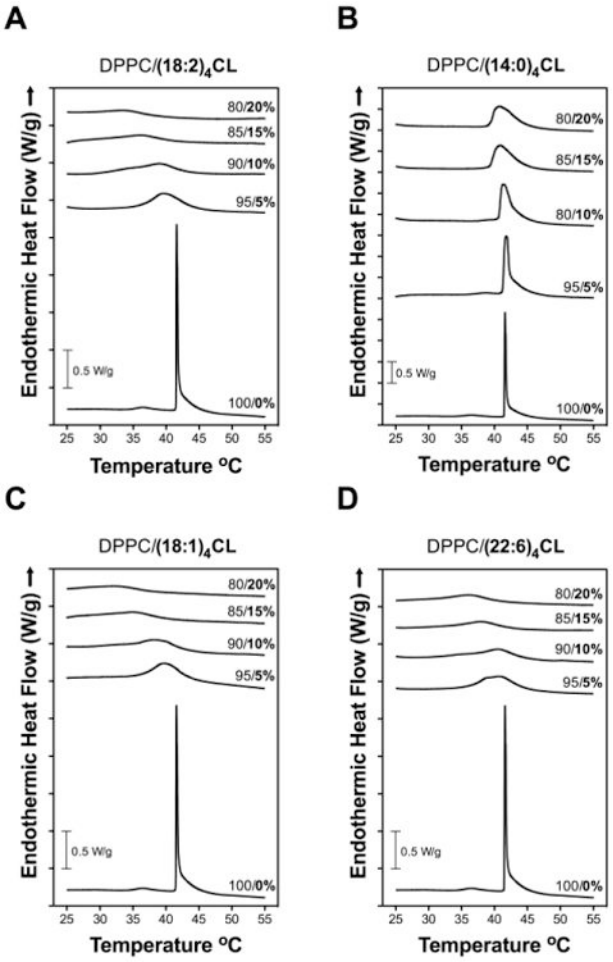

Figure 5. $(14:0)_4$CL does not lower the main phase transition temperature of DPPC as effectively as other CL species

DSC heating scans for DPPC with differing levels of (A) $(18:2)_4$CL, (B) $(14:0)_4$CL, (C) $(18:1)_4$CL, and (D) $(22:6)_4$CL. Values to the right indicate the mol percent of DPPC/CL. No hysteresis was observed since nearly identical results were observed for cooling scans. Data are single scans representative of 3 independent experiments.

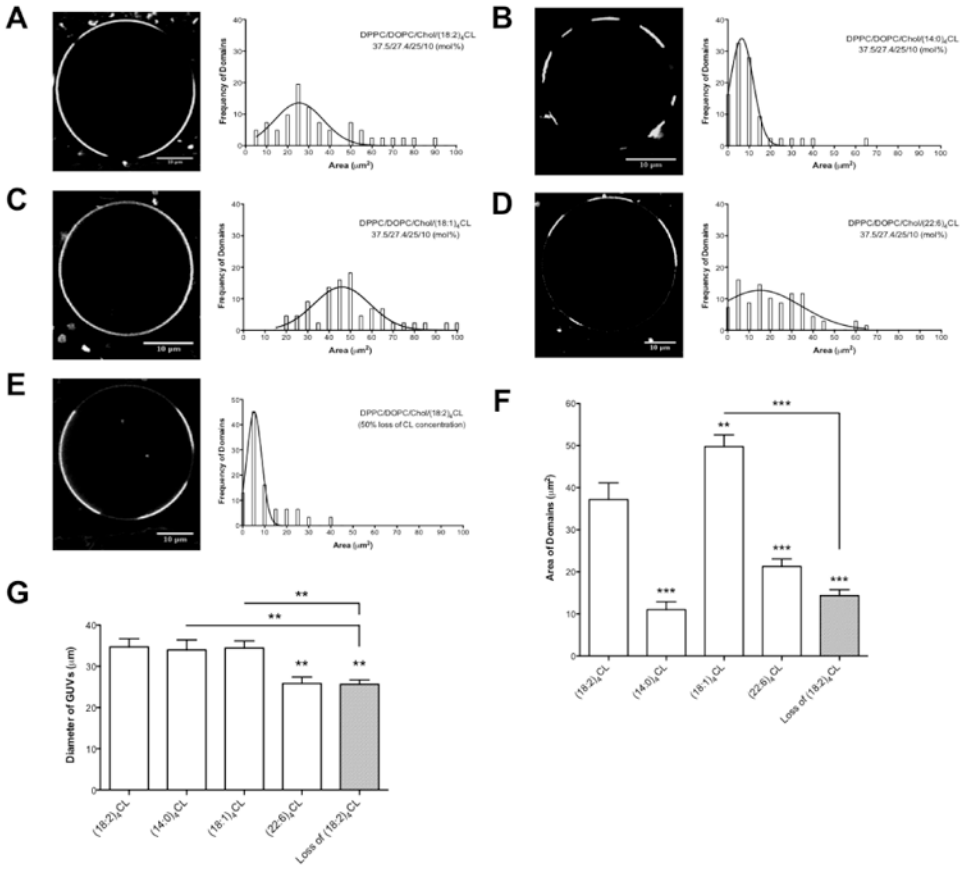

Figure 6. Loss of $(18:2)_4$CL content and CL acyl chain composition have differential effects on GUV lipid microdomain organization

Sample images of DPPC/DOPC/Chol/CL (37.5/27.4/25/10 mol%) containing either (A) $(18:2)_4$CL, (B) $(14:0)_4$CL, (C) $(18:1)_4$CL, or (D) $(22:6)_4$CL. Plots to the right of the images indicate the frequencies of domains as a function of domain area (μm^2). (E) Sample GUV image of DPPC/DOPC/Chol/$(18:2)_4$CL with a 50% loss of CL concentration. (F) The average microdomain area is plotted for the differing CL species and upon the loss of CL content. (G) Average diameter of the GUVs analyzed. Data are from a total of 40-60 GUVs analyzed from 2-3 independent experiments. Data are average ± S.E.M. Asterisks indicate significance from $(18:2)_4$CL, unless otherwise noted: **P<0.01, ***P<0.001.

Table 1

Excess area/molecule, elasticity modulus, and Gibbs free energy of mixing in response to decreasing CL content in simple and complex lipid mixtures

Values were calculated from pressure-area isotherms at a physiologically relevant surface pressure of 30 mN/m. Data are average ± S.E.M. from 3-6 independent experiments.

Lipid Mixture	Excess Area/Molecule (Å^2)	C_s^{-1} (mN/m)	ΔG_{mix} (kJ/mol)
DPPC/**(18:2)$_4$CL** (80/**20** mol%)[a]	-0.2 ± 0.8	69.1 ± 0.7	-1.8 ± 0.0
DPPC/**(18:2)$_4$CL** (90/**10** mol%)[b]	-1.2 ± 0.9	70.9 ± 1.7	-0.6 ± 0.0
DPPC/(18:2)$_4$CL (50% loss of CL concentration)[c]	-11.2 ± 0.7	58.0 ± 1.9	-0.9 ± 0.0
DOPC/DOPE/**(18:2)$_4$CL**/DOPS/Chol (40/30/**20**/5/5 mol%)[a]	1.8 ± 1.1	87.7 ± 3.1	-3.5 ± 0.4
DOPC/DOPE/**(18:2)$_4$CL**/DOPS/Chol (46/33/**10**/5.5/5.5 mol%)[b]	0.5 ± 1.5	94.7 ± 1.2	-3.5 ± 0.0
DOPC/DOPE/(18:2)$_4$CL/DOPS/Chol (50% of CL concentration)[c]	-4.2 ± 0.9	79.0 ± 2.9	-3.9 ± 0.1

[a] represents the control.

[b] represents the ‘compensated loss’ of CL, which is defined as decreasing CL content by 50 mol% at the expense of increasing other phospholipids in the mixture.

[c] represents the ‘absolute loss’ of CL, which is defined as 50% loss of CL concentration relative to the control.

Table 2

Excess area/molecule, elasticity modulus, and Gibbs free energy of mixing for CLs of differing acyl chain composition in simple and complex lipid mixtures

Values were calculated from pressure-area isotherms at a physiologically relevant surface pressure of 30 mN/m. Data are average ± S.E.M. from 3-9 independent experiments.

Lipid Mixture	Excess Area/Molecule (Å^2)	C_s^{-1} (mN/m)	Δ_{Gmix} (kJ/mol)
DPPC/**(18:2)$_4$CL** (80/**20** mol%)[a]	-0.2 ± 0.8	69.1 ± 0.7	-1.8 ± 0.0
DPPC/**(14:0)$_4$CL** (80/**20** mol%)	3.9 ± 0.4	194.2 ± 16.1	-1.1 ± 0.0
DPPC/**(18:1)$_4$CL** (80/**20** mol%)	0.4 ± 0.7	71.1 ± 4.1	-1.1 ± 0.1
DPPC/**(22:6)$_4$CL** (80/**20** mol%)	-6.4 ± 0.8	47.9 ± 0.6	-0.8 ± 0.1
DOPC/DOPE/**(18:2)$_4$CL**/DOPS/Chol (40/30/**20**/5/5 mol%)[a]	1.8 ± 1.1	87.7 ± 3.1	-3.5 ± 0.4
DOPC/DOPE/**(14:0)$_4$CL**/DOPS/Chol (40/30/**20**/5/5 mol%)	10.7 ± 0.6	96.3 ± 0.7	-4.1 ± 0.0
DOPC/DOPE/**(18:1)$_4$CL**/DOPS/Chol (40/30/**20**/5/5 mol%)	-0.5 ± 0.9	98.0 ± 1.3	-3.3 ± 0.2
DOPC/DOPE/**(22:6)$_4$CL**/DOPS/Chol (40/30/**20**/5/5 mol%)	-0.3 ± 0.5	74.4 ± 2.9	-4.1 ± 0.1

[a] represents the control.

Table 3

Thermodynamic profiles of DPPC lipid bilayers in the presence of differing CL species

Data are from heating scans of DPPC with increasing mol percent CL. Data are average ± S.E.M. from 3 independent experiments.

CL	DPPC/CL (mol%)	T_m (°C)	$T_{m1/2}$ (°C)	ΔH (kJ/mol)
----	100/**0**	41.6 ± 0.0	0.24 ± 0.0	46.1 ± 0.7
$(18:2)_4$	95/**5**	40.0 ± 0.2	5.3 ± 0.1	40.1 ± 3.1
	90/**10**	38.6 ± 0.2	8.9 ± 0.5	34.7 ± 0.9
	85/**15**	37.1 ± 0.3	6.8 ± 0.2	22.3 ± 0.9
	80/**20**	34.8 ± 0.1	7.2 ± 0.8	19.1 ± 5.3
$(14:0)_4$	95/**5**	41.7 ± 0.1	0.8 ± 0.0	71.3 ± 2.5
	90/**10**	41.4 ± 0.1	1.9 ± 0.2	77.0 ± 1.6
	85/**15**	41.1 ± 0.1	3.2 ± 0.1	69.4 ± 1.2
	80/**20**	41.1 ± 0.1	3.7 ± 0.1	64.3 ± 3.4
$(18:1)_4$	95/**5**	39.9 ± 0.1	5.5 ± 0.1	52.5 ± 1.0
	90/**10**	38.7 ± 0.2	7.8 ± 0.5	31.3 ± 3.5
	85/**15**	35.9 ± 0.1	6.6 ± 0.2	16.8 ± 1.8
	80/**20**	32.7 ± 0.2	10.3 ± 1.8	30.9 ± 7.2
$(22:6)_4$	95/**5**	40.9 ± 0.1	6.0 ± 0.1	43.2 ± 1.5
	90/**10**	40.2 ± 0.2	6.8 ± 0.3	33.2 ± 2.8
	85/**15**	38.2 ± 0.1	6.5 ± 0.1	21.4 ± 0.8
	80/**20**	36.7 ± 0.2	6.9 ± 0.3	20.4 ± 3.3